INORGANIC CHEMISTRY FRONTIERS

RESEARCH ARTICLE

View Article Online
View Journal | View Issue

Cite this: *Inorg. Chem. Front.*, 2025, **12**, 6503

Speciation and structural transformation of a V^V–malate complex in the absence and in the presence of a protein: from a dinuclear species to decavanadate†

Maddalena Paolillo, [a] Giarita Ferraro, [a] Nadiia I. Gumerova, [b] Federico Pisanu, [c] Eugenio Garribba, *[c] Annette Rompel *[b] and Antonello Merlino *[a]

A strategy for the development of new vanadium-based drugs is the preparation of complexes that target proteins and bear molecules involved in the cellular metabolism as ligands, like α-hydroxycarboxylic acids. Based on these premises, this study explores the solution behaviour of the dioxidovanadium(V) complex of malic acid, $Cs_2[V^V_2O_4(mal)_2]\cdot 2H_2O$, and its interaction with the model protein lysozyme (HEWL) at room and at physiological temperature using ^{51}V nuclear magnetic resonance (NMR), electrospray ionisation-mass spectrometry (ESI-MS) and X-ray crystallography. The results show the coexistence in aqueous solution of various molecular species containing two or ten V^V centres. In solution these species are formed regardless of the presence of HEWL, while at 37 °C the formation of $[V^V_{10}O_{28}]^{6-}$ (V_{10}) is precluded when the protein is present. Crystallographic data reveal that, when protein crystals are incubated with the V compound at room temperature (25 °C) and at pH 4.0, $[V^{IV}O]^{2+}$, $[V^V_2O_5(mal)]^{2-}$, $[V^V_{10}O_{26}]^{2-}$ and $[V^V_{10}O_{28}]^{6-}$ are bound to the protein, while at 37 °C, under the same conditions, only $[V^{IV}O]^{2+}$ interacts with HEWL. $[V^V_{10}O_{28}]^{6-}$ can bind the protein both covalently (as $[V^V_{10}O_{26}]^{2-}$ ion) and non-covalently. Whereas the transformation of $[V^V_2O_4(mal)_2]^{2-}$ to $[V^V_2O_5(mal)]^{2-}$ is expected on the basis of thermodynamic considerations, the formation of V_{10} and of the V_{10}–HEWL adduct is not easily predictable. Docking calculations confirm the experimental results and highlight the role of protein–protein interaction in the stabilization of the revealed adduct. This study demonstrates that vanadium compounds can undergo transformation in solution, giving rise to species that interact with proteins through several binding modes and stabilization mechanisms.

Received 26th June 2025,
Accepted 19th July 2025

DOI: 10.1039/d5qi01384d

rsc.li/frontiers-inorganic

Introduction

Vanadium-based drugs have been proposed for treating various diseases, in particular diabetes and several forms of cancer.[1–15] A valuable strategy for the design of new drugs is the synthesis of metal complexes with natural or bioactive ligands, for example compounds involved in the cellular metabolism.[16,17] α-Hydroxycarboxylic acids are ubiquitous in nature and play key roles in different cellular pathways such as the Krebs cycle (citrate, isocitrate, malate), the Cori cycle (lactate) and photorespiration (glycolate),[18,19] representing good candidates for this approach. Due to the importance of both vanadates and α-hydroxycarboxylic acids, the mutual interaction of these groups of compounds was intensively studied.[18–23] Among the α-hydroxycarboxylic acids, malic acid stands out as a promising candidate; it is found in apples and other fruits, and in humans.[24] Moreover, malic acid is used as a taste enhancer and acidulant, frequently in conjunction with citric acid.[25] It functions as a chelating and buffering ingredient in cleaning and personal care products.[25] Additional uses of malic acid include the pharmaceutical industry, such as a component of the migraine medication almotriptan malate,[25] in the manufacturing of semiconductors as a polishing or cleaning formulation compound,[25,26] as an additive for animal feed,[25] and as a component of mixtures with low transition temperatures.[25,27,28] Malic acid is also a good building block for the synthesis of homo- and heteropolymers due to its dicarboxylic nature.[25]

[a]*Department of Chemical Sciences, University of Naples Federico II, Complesso Universitario di Monte Sant'Angelo, Via Cintia, I-80126 Napoli, Italy. E-mail: antonello.merlino@unina.it*
[b]*Universität Wien, Fakultät für Chemie, Institut für Biophysikalische Chemie, 1090 Wien, Austria. E-mail: annette.rompel@univie.ac.at; https://www.bpc.univie.ac.at*
[c]*Dipartimento di Medicina, Chirurgia e Farmacia, Università di Sassari, Viale San Pietro, I-07100 Sassari, Italy. E-mail: garribba@uniss.it*
† Electronic supplementary information (ESI) available. See DOI: https://doi.org/10.1039/d5qi01384d

Proteins are one of the primary targets for vanadium complexes (VCs), playing a major role in their biospeciation and biotransformation within the body[10,29,30] and their mechanism of action.[9,31–34] The interaction of selected VCs with small model proteins like hen egg white lysozyme (HEWL), myoglobin, ubiquitin, and bovine pancreatic ribonuclease has been investigated using electrospray ionization-mass spectrometry (ESI-MS), electron paramagnetic resonance (EPR), computational studies (docking, DFT, QM/MM), UV-visible spectroscopy, circular dichroism (CD), fluorescence spectroscopy, and X-ray crystallography.[29,30,34–56] The whole VCs or V-containing fragments formed in solution are the result of hydrolysis, redox, and ligand exchange reactions and the administered VC or its fragments can bind proteins covalently or non-covalently.[10,33,34,57] These processes can also lead to the formation of polyoxidovanadates (POVs), a subclass of polyoxidometalates (POMs) known for their structural diversity and reactivity in biological and aqueous environments.[58–60] Interactions with proteins are key points in the comprehension of the transport, activity and mechanism of action of V-based drugs and the consequences could be different depending on the protein involved and type of established interaction: for example, the binding of V^{V} (and V^{IV}) compounds to human transferrin (hTF) can reduce their uptake and cytotoxicity on some cell lines due to return of $V^{IV/V}$–hTF species to the surface of the cells after the endosomal step,[61] while the formation of adducts between VCs and human serum albumin can result in an increase of their antiproliferative action.[62]

Here, we studied the in-solution behaviour at room and physiological temperatures and the interaction with HEWL of the dioxidovanadium(V) complex of malic acid (abbreviated with mal), dicaesium bis((μ$_2$-malato)-dioxidovanadium(V)) dihydrate ($Cs_2[V^{V}_2O_4(mal)_2]\cdot 2H_2O$, Fig. 1). The aims of this work are: (i) the characterization of the VC–HEWL adducts, where VC is the complex $[V^{V}_2O_4(mal)_2]^{2-}$ or a V-containing fragment derived upon its dissociation and transformation, through a combined application of instrumental techniques such as ^{51}V nuclear magnetic resonance (NMR), ESI-MS and X-ray crystallography; (ii) the determination of the type of binding, covalent or non-covalent; (iii) the comparison of the adducts formed at room (RT, 25 °C) and physiological temperature (37 °C); (iv) the use of docking calculations to predict the binding sites and determine the factors stabilizing the VC–HEWL adducts.

The understanding of the biospeciation and biotransformation of vanadium compounds within the body and of the interaction with proteins, which – due to the large abundance in the extra- and intracellular environment – represent the primary interactors for VCs, could improve the comprehension of the mechanisms at the basis of their multiple biological activities.

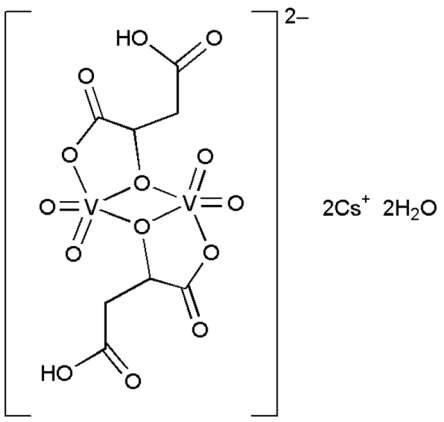

Fig. 1 Structure of $Cs_2[V^{V}_2O_4(mal)_2]\cdot 2H_2O$.

Materials and methods

Materials

D,L-Malic acid, Cs_2CO_3, V_2O_5 and other reagents for both the synthetic and reactivity studies were purchased from Sigma-Aldrich and used without further purification. HEWL was also purchased from Sigma-Aldrich and used without further purification.

Synthesis

V_2O_5 (1 mmol, 0.182 g) and Cs_2CO_3 (1.1 mmol, 0.358 g) were dissolved in water (5 mL) and the reaction mixture was heated for 1 h to 40 °C while stirring. The solution, with a pH in the range 3.0–4.0, was cooled in an ice bath and malic acid (2 mmol, 0.268 g) was progressively added. At RT, a solid was formed. This was filtered, washed with a small amount of EtOH and air-dried at RT. $Cs_2[V^{V}_2O_4(mal)_2]\cdot 2H_2O$: anal. calc. for $C_8H_{12}Cs_2O_{16}V_2$: C, 13.13; H, 1.65; H_2O, 4.9; $Cs_2O + V_2O_5$: 61.2%. Found: C, 13.24; H, 1.68; H_2O, 5.0; $Cs_2O + V_2O_5$, 61.0%.

Physical measurements

Elemental analyses (C, H, N) were obtained with a Perkin–Elmer 240 B elemental analyzer. Thermogravimetric data were obtained with a Perkin–Elmer TGS-2 apparatus in air or under a nitrogen flow. IR spectra were recorded with a JASCO FT/IR-480Plus spectrometer using KBr pellets (4000–600 cm^{-1}).

^{51}V NMR studies

^{51}V NMR spectra of the $Cs_2[V^{V}_2O_4(mal)_2]\cdot 2H_2O$ (concentration = 5 mM) in D_2O, and in 1.1 M sodium chloride, 0.1 M sodium acetate pH 4.0 and 10% D_2O, in the absence and in the presence of HEWL (concentration = 13 mg mL^{-1}) were recorded. Spectra have been collected after 1 hour and 7 days of incubation at RT and after 42 hours and 7 days of incubation at 37 °C. NMR spectra were recorded on an Avance Neo 500 MHz FT-NMR spectrometer (Bruker, Rheinstetten, Germany) at 25 °C. Chemical shifts were measured relative to $V^{V}OCl_3$ and are given in parts per million (ppm, δ). The ^{51}V NMR samples were recorded at 131.60 MHz (2000 scans, accumulation time 0.05 s, relaxation delay 0.01 s). Spectra were analysed using MestReNova with Automatic Phase Correction and using Whittaker Smoother as baseline.

Mass spectrometry

Mass spectra of the $Cs_2[V^V_2O_4(mal)_2]\cdot 2H_2O$ (concentration ~100 μM) were collected in H_2O, and acetonitrile/methanol + 1% H_2O in positive and negative mode on timsTOF flex LC-MS System supplied by Bruker Daltonics Ltd. The spectra were recorded in positive and negative ion mode within the *m*/*z* range of 90 to 600, and the spectrometer was calibrated using the standard tunemix (Bruker Daltonik GmbH, timsTOF Pro User Manual, Bremen, Germany) to ensure an accuracy of approximately 5 ppm in the *m*/*z* region of 50–1800. Spectra were analysed using Bruker Daltonics Data Analysis 4.0 software. Other settings: capillary voltage, 2500 V; nebulizer, 0.3 Bar; dry gas flow, 3.0 L min^{-1} (nitrogen); dry heater temperature, 200 °C; flow rate, 3 μL min^{-1}.

Mass spectra of HEWL (concentration = 13 mg mL^{-1} in distilled water) in the absence and in the presence of the $Cs_2[V^V_2O_4(mal)_2]\cdot 2H_2O$ (ratio 1 : 1) were collected after diluting the sample 1 : 100 in acetonitrile/H_2O 9/1 + 1% formic acid (FA) in positive mode on timsTOF flex LC-MS System supplied by Bruker Daltonics Ltd. Spectra were deconvoluted using MagTran software. Other settings: capillary voltage, 3500 V; nebulizer, 0.3 Ba; dry gas flow, 3.0 L min^{-1} (nitrogen); dry heater temperature, 200 °C; mass range, 300–3000 *m*/*z*.

Crystallization and data collection

HEWL (13 mg mL^{-1}) was crystallized using the hanging drop vapor diffusion method and 1.1 M sodium chloride and 0.1 M sodium acetate pH 4.0 as a reservoir. The reservoir solution had a volume of 500 μL, while the drop was 2 μL. Crystals formed within one day at 20 °C. Pre-grown HEWL crystals were then soaked in stabilizing solutions containing the mother liquor saturated with $Cs_2[V^V_2O_4(mal)_2]\cdot 2H_2O$ for 7 days. After treatment with $Cs_2[V^V_2O_4(mal)_2]\cdot 2H_2O$, the HEWL crystals were cryopreserved for X-ray diffraction by transferring them into a solution consisting of 75% reservoir solution and 25% glycerol. The crystals were then fished using a nylon loop, rapidly cooled in liquid nitrogen, and shipped to synchrotrons. X-ray diffraction data were collected from two crystals at the XRD2 beamline of the Elettra synchrotron (Trieste, Italy) at 100 K, using a wavelength of 1.00 Å. The crystals diffracted X-rays to 1.46 Å and 1.18 Å resolution, respectively, at 100 K.

HEWL (100 mg mL^{-1}) was also crystallized at 37 °C using the hanging drop vapour diffusion method under the same crystallization condition. Crystals were grown within a few hours. Pre-formed HEWL crystals were then exposed to stabilizing solutions containing the mother liquor saturated with $Cs_2[V^V_2O_4(mal)_2]\cdot 2H_2O$ for a soaking time of a few hours at 37 °C. X-ray diffraction data were collected from one crystal at the XRD2 Beamline of the Elettra synchrotron (Trieste, Italy) at 37 °C, using a wavelength of 1.00 Å. The crystal diffracted X-rays to 2.09 Å resolution. Data processing and scaling were performed using the Global Phasing autoPROC pipeline.[63] Data collection statistics are presented in Table S1.†

Structure solution and refinement

The structures were solved by using the molecular replacement method implemented in the Phaser program from CCP4 suite,[64] and the structure from Protein Data Bank (PDB) with entry 193L[65] as a template. Refinement was carried out using Refmac5.[66] To confirm the presence of vanadium atoms, 2Fo–Fc, Fo–Fc and anomalous difference electron density maps were inspected using Coot.[67] Ligand positions were restrained to facilitate geometry optimization. The final models refine to *R*-factor and *R*free values in the range of 0.191–0.239 and 0.235–0.312 (Table S1†). Figures were generated using PyMOL (**https://www.pymol.org**). Coordinates and structure factors were deposited in the PDB under the accession codes 9RBG, 9RBT and 9RBV.

Docking calculations

Dockings were run with the software GOLD 2024.2.0 of the Cambridge Crystallographic Data Centre (CCDC).[68] Two approaches were adopted, one consisting of docking at one HEWL chain, referred herein as "classic", and another consisting of docking at the interface between two HEWL symmetry mates in the crystal lattice, referred as "symmetry mate" approach.[44] For the "classic" method, an ensemble docking was performed, using the HEWL structures with PDB codes 2LYZ,[69] 8RTJ,[44] 8RTK,[44] and the crystallographic structures **A** and **B** reported in this work (PDB codes 9RBG and 9RBT). Concerning the "symmetry mate" method, the docking was based on the two protein chains from crystallographic structures with codes 9RBG and 9RBT.

Where vanadium–protein covalent bonds were experimentally observed, covalent dockings were performed. Dummy hydrogen atoms were used to simulate vacant coordinative positions around the vanadium centre, following the method proposed in the literature for the study of covalent adducts with GOLD software.[70,71]

The models of $[V^V_{10}O_{28}]^{6-}$, $[V^V_{10}O_{26}]^{2-}$, and $[V^V_2O_5(mal)]^{2-}$ were obtained from the crystallographic structures. For the covalent dockings, the dummy hydrogen atoms in $[V^V_{10}O_{26}]^{2-}$ took the place of the protein atoms bound to the V centre. V–(dummy hydrogen) distances were set to 0.75 Å.

Crystallographic water molecules, ions and possible small ligands were removed from the structures in the first series of calculations. Protonation states of Asp, Glu and His at pH 4.0 were calculated using H++.[72]

For the ensemble docking of the "classic" approach, the calculations were performed on an evaluation space defined by a 30 Å radius sphere which allows exploring all the protein. For the "symmetry mate" approach, the binding sites were defined close to the observed binding.

All non-covalent dockings were rigid, while the covalent dockings comprehended some degree of flexibility: in the docking of $[V^V_{10}O_{26}]^{2-}$ with the "symmetry mate" approach, the side chains of Lys1, Glu7, and Arg14 of both the symmetry mate chains were set free to move; in the docking of $[V^{IV}O]^{2+}$ free movement of Arg14, His15, Asp18, and Asn19 side chains

in the five protein structures of the ensemble was allowed. For $[V^{V}_{2}O_5(mal)]^{2-}$, an additional docking was performed by keeping a $[V^{V}_{2}O_5(mal)]^{2-}$ ion in the binding site, two Na^+ ions and fourteen crystallographic waters near the binding site.

GoldScore[68] was set as the scoring function, with which the *Fitness* score parameter (*F*) – used for ranking the solutions – was calculated. 100 runs of genetic algorithm (GA) were performed for each calculation. The minimum number of operations was set to 100 000. Solutions were analysed through the *F* score and clustered according to the root mean square deviation (rmsd) of the atomic coordinates. Each cluster, representing a docking pose, contained solutions with rmsd values within 2.5 Å. Figures were generated with UCSF Chimera 1.18.[73]

Results and discussion

Solution behaviour of $Cs_2[V^{V}_{2}O_4(mal)_2]\cdot 2H_2O$ in the absence and in the presence of HEWL: ^{51}V NMR studies

First, we investigated the behaviour of $Cs_2[V^{V}_{2}O_4(mal)_2]\cdot 2H_2O$ in solution by collecting ^{51}V NMR spectra of the compound (concentration = 5 mM) in D_2O, and applying the condition used to grow crystals of HEWL followed by treatment with the V compound (1.1 M sodium chloride, 0.1 M sodium acetate pH 4.0 and 10% D_2O, see below) in the absence and in the presence of the protein (concentration = 13 mg mL^{-1}) (Fig. 3 and 4). Spectra were collected after 1 hour and 7 days of incubation at RT (Fig. 3), and after 42 hours and 7 days of incubation at 37 °C (Fig. 4).

The solution behaviour of the systems containing vanadium(V) and α-hydroxycarboxylates has been extensively studied by ^{51}V NMR.[18,21,22,74–77] These spectra reveal several complexes, the major species being $[V^{V}_{2}O_4(mal)_2]^{2-}$ and $[V^{V}_{2}O_5(mal)]^{2-}$. The high stability of the dinuclear, and even trinuclear, compounds was demonstrated for some α-hydroxycarboxylates, for example for lactate (lact) and mandelate.[18,77] The bridge can be broken upon reaction with reductants, like cysteine, which reduces $[V^{V}_{2}O_4(lact)_2]^{2-}$ completely after less than 2 h.[78] $[V^{V}_{2}O_4(mal)_2]^{2-}$ consists of two coordination equivalent centres, characterized by a signal at around −533 ppm, while $[V^{V}_{2}O_5(mal)]^{2-}$ shows two non-equivalent V centres (signals at −551 ppm and at −533 ppm). Additional signals are observed at −561 ppm, attributed to $H_2V^{V}O_4^-$ (V_1), at −574 ppm, arising from $H_2V^{V}_{2}O_7^{2-}$ (V_2), at −579 ppm, due to $V^{V}_{4}O_{12}^{4-}$ (V_4). Signals at the regions −525 to −514 ppm, −507 to −497 ppm, and −425 to −423 correspond respectively to the V_A, V_B, and V_C centres of $[H_xV^{V}_{10}O_{28}]^{(6-x)-}$ (V_{10}, x = 0–3) (Fig. 2). These chemical shifts vary depending on the protonation state of the decavanadate species. Signals at approximately −517 and −502 ppm have also been attributed to $[V^{V}O_2(mal)(H_2O)]^-$ and $[V^{V}O_2(mal)(OH)]^{2-}$, respectively.[18,21,22,74–77,79,80]

The spectra of $Cs_2[V^{V}_{2}O_4(mal)_2]\cdot 2H_2O$ solutions collected at RT reveal the presence of $[V^{V}_{2}O_4(mal)_2]^{2-}$ (signal at ~−534 ppm), $[V^{V}_{2}O_5(mal)]^{2-}$ (signals at ~−538 ppm and −545 ppm), V_{10} (signals at ~−425 ppm, −502 ppm, and −520 ppm) under all investigated experimental conditions.

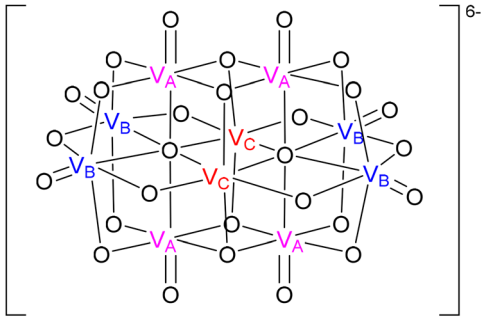

Fig. 2 V_A, V_B, and V_C centres in $[V^{V}_{10}O_{28}]^{6-}$.

Peak integration analysis suggests that the percentage of decavanadate in the various solutions increases over time. A small amount (~1%) of V_{10} is also observed in the presence of the protein (Fig. 3, and Table S2†).

The spectra collected at 37 °C show similar results and suggest the presence in solution of $[V^{V}_{2}O_4(mal)_2]^{2-}$ (signal at ~−534 ppm), $[V^{V}_{2}O_5(mal)]^{2-}$ (signals at ~−538 and −545 ppm), and V_{10} (signals at ~−425 ppm, −502 ppm, and −520 ppm) also at physiological temperature. Notably, under these conditions, the percentage of the decavanadate increases after 7 days of incubation in the absence of protein, while its formation is precluded at 37 °C in the presence of HEWL (Fig. 4, and Table S3†). This is in contrast with recent results indicating that HEWL could stabilize decavanadate and other larger POVs, like V_{15} and V_{20}, also at physiological temperature.[38,43,81,82]

Solution behaviour of $Cs_2[V^{V}_{2}O_4(mal)_2]\cdot 2H_2O$ in the absence and in the presence of HEWL: mass spectrometry data

The behaviour of the $Cs_2[V^{V}_{2}O_4(mal)_2]\cdot 2H_2O$ was investigated by collecting mass spectra of the compound in H_2O, and acetonitrile/methanol + 1% H_2O, a mixture that ensures a good ionization, applying ESI-MS both in positive (Fig. S1†) and in negative mode (Fig. S2†).

The negative-ion mode spectrum of $Cs_2[V^{V}_{2}O_4(mal)_2]\cdot 2H_2O$ in H_2O is shown in Fig. S2A.† A series of singly charged and doubly charged species are detected. The singly charged series include protonated and unprotonated vanadates $[V^{V}O_3]^-$, $[H_2V^{V}O_4]^-$, $[V^{IV}V^{V}O_5]^-$, $[HV^{V}_{2}O_6]^-$ and $[V^{V}_{3}O_8]^-$, the monoanionic malate ligand $[C_4H_5O_5]^-$ (*i.e.*, $[mal^{2-} + H^+]^-$) and various vanadium complexes with one or two V centres: $[V^{V}O_2(mal)]^-$, $[V^{V}_{2}O_4(mal) - H^+]^-$, and $[V^{V}_{2}O_4(mal)(H_2O) - H^+]^-$. The only doubly charged species identified contains two V centres: $[V^{V}_{2}O_5(mal)]^{2-}$. Additionally, $[V^{V}_{10}O_{26}]^{2-}$, a decavanadate anion with two oxido ligands less than usual $[V^{V}_{10}O_{28}]^{6-}$, has been observed (Table 1). The negative-ion mode spectrum of $Cs_2[V^{V}_{2}O_4(mal)_2]\cdot 2H_2O$ in acetonitrile/methanol + 1% H_2O is shown in Fig. S2B.† In this spectrum, most of the species present in water were observed (Table 1) with the important exception that decavanadate ($[V^{V}_{10}O_{26}]^{2-}$) is missing.

The positive-ion mode ESI-MS spectrum of HEWL (concentration = 13 mg mL^{-1}) diluted 1 : 100 in acetonitrile/H_2O + 1% FA was recorded. To determine the exact mass of the protein,

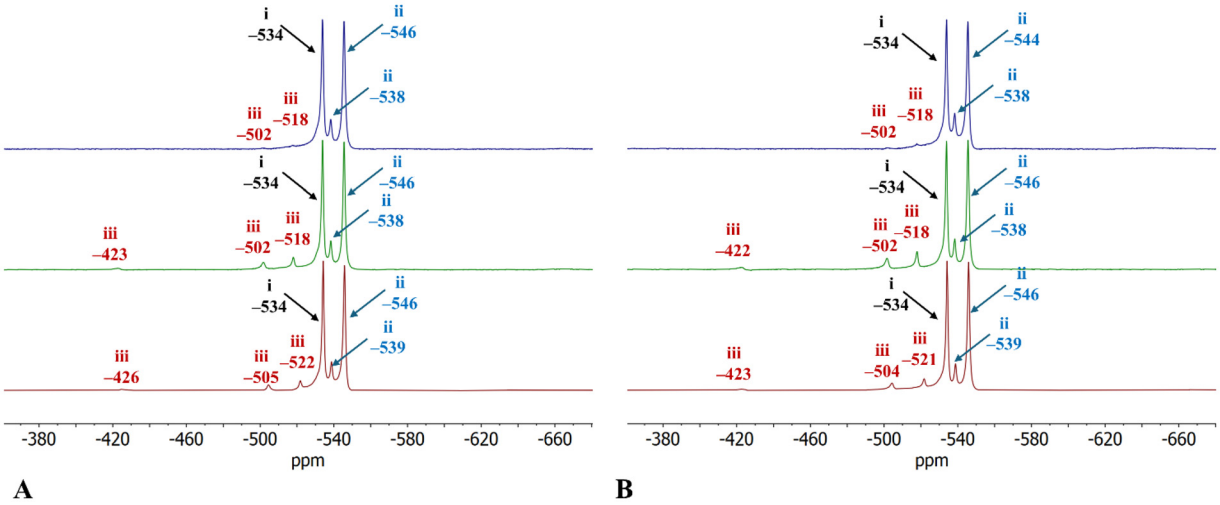

Fig. 3 ^{51}V NMR spectra measured at RT after 1 h (A) and 7 d (B) of incubation of $Cs_2[V^V_2O_4(mal)_2]\cdot 2H_2O$ (5 mM) dissolved in D_2O (red lines); in 1.1 M sodium chloride, 0.1 M sodium acetate pH 4.0 and 10% D_2O (green lines); and in 1.1 M sodium chloride, 0.1 M sodium acetate pH 4.0 and 10% D_2O in presence of HEWL (13 mg mL^{-1}) (blue lines). "i" indicates $[V^V_2O_4(mal)_2]^{2-}$, "ii" indicates $[V^V_2O_5(mal)]^{2-}$ and "iii" the decavanadate anion V_{10}.

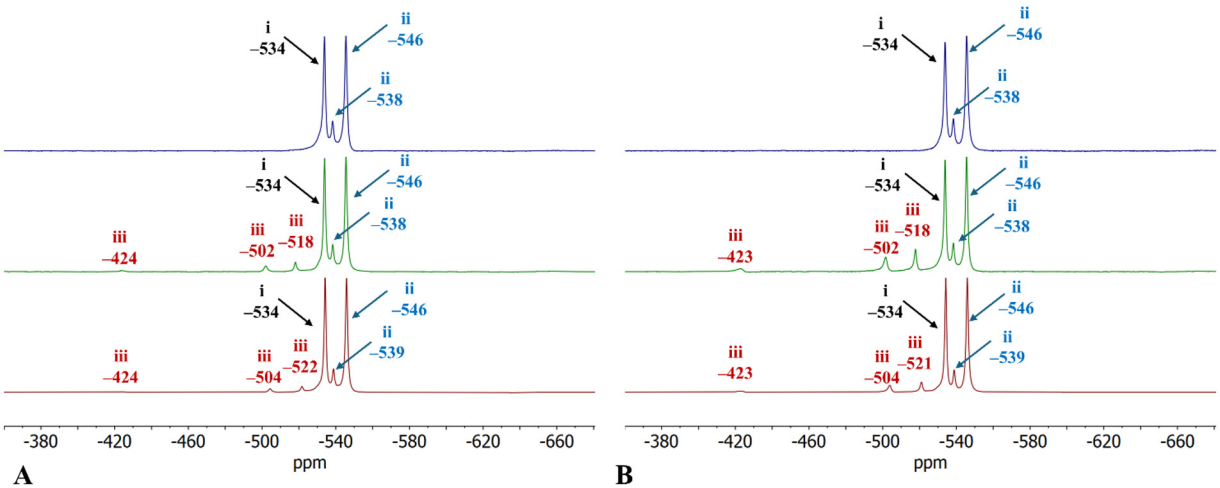

Fig. 4 ^{51}V NMR spectra measured at 37 °C after 42 h (A) and 7 d (B) of incubation of $Cs_2[V^V_2O_4(mal)_2]\cdot 2H_2O$ (5 mM) dissolved in D_2O (red lines); in 1.1 M sodium chloride, 0.1 M sodium acetate pH 4.0 and 10% D_2O (green lines); and in 1.1 M sodium chloride, 0.1 M sodium acetate pH 4.0 and 10% D_2O in presence of HEWL (13 mg mL^{-1}) (blue lines). "i" indicates $[V^V_2O_4(mal)_2]^{2-}$, "ii" indicates $[V^V_2O_5(mal)]^{2-}$ and "iii" the decavanadate anion V_{10}.

the spectrum was deconvoluted using MagTran software, which estimates protein mass from mass-to-charge spectra consisting of multiple peaks corresponding to multiply charged ions. The result is reported in Fig. 5A, where an intense central peak at 14304.9 Da is observed.

The positive-ion mode ESI-MS spectrum recorded after dissolving HEWL in the presence of $Cs_2[V^V_2O_4(mal)_2]\cdot 2H_2O$ (VC : HEWL molar ratio = 1 : 1) diluted 1 : 100 in acetonitrile/H_2O + 1% FA is reported in Fig. 5B. The spectrum shows two intense peaks at 14304.9 Da (metal-free protein) and at 15268.2 Da, the latter attributed to the $[H_6V^V_{10}O_{28}]$–HEWL adduct. This result confirms the presence of decavanadate in solution under the used experimental conditions. Literature data indicate that, in acetonitrile, the predominant vanadate species is the most acidic one.[83] Therefore, in the case of decavanadate, the protonated species $[H_6V^V_{10}O_{28}]$ is expected to be the dominant form.

Interaction of HEWL with $Cs_2[V^V_2O_4(mal)_2]\cdot 2H_2O$: crystallographic studies at cryogenic temperature

X-ray diffraction data have then been collected at 100 K on two crystals of HEWL grown in 1.1 M sodium chloride and 0.1 M sodium acetate at pH 4.0 and exposed for 7 days to $Cs_2[V^V_2O_4(mal)_2]\cdot 2H_2O$ powder at RT (Table S1†). These crystals diffracted to 1.46 Å and 1.18 Å resolution, respectively, and belong to the space group $P4_32_12$, with one single protein molecule in the asymmetric unit (Fig. 6). The overall structures of the protein in the two crystals are very similar to each other,

Table 1 Experimental and calculated *m/z* values for $Cs_2[V^V_2O_4(mal)_2]\cdot 2H_2O$ dissolved in H_2O and in ACN/MeOH + 1% H_2O, recorded in negative ion mode using ESI-MS

Observed species	Experimental *m/z*	Simulated *m/z*
In H_2O		
$[V^VO_3]^-$	98.93	98.93
$[H_2V^VO_4]^-$	116.94	116.94
$[mal^{2-} + H^+]^-$	133.01	133.01
	134.02	134.02
$[V^V_2O_5(mal)]^{2-}$	156.93	156.93
	157.44	157.44
	157.94	157.94
$[V^{IV}V^VO_5]^-$	181.86	181.86
$[HV^V_2O_6]^-$	198.87	198.87
$[V^VO_2(mal)]^-$	214.94	214.94
	215.94	215.94
$[V^V_3O_8]^-$	280.79	280.79
$[V^V_2O_4(mal) - H^+]^-$	296.87	296.87
	297.87	297.87
$[V^V_2O_4(mal)(H_2O) - H^+]^-$	314.88	314.88
	315.88	315.88
$[V^V_2O_5(mal)^{2-} + Na^+]^-$	336.86	336.86
	337.86	337.86
$[V^V_2O_5(mal)^{2-} + Cs^+]^-$	446.77	446.77
	447.78	447.78
$[V^V_{10}O_{26}]^{2-}$	462.16	462.16
	462.65	462.65
	463.16	463.16
	463.66	463.66
	464.16	464.16
	464.65	464.65
In ACN/MeOH + 1% H_2O		
$[V^VO_3]^-$	98.93	98.93
$[H_2V^VO_4]^-$	116.94	116.94
$[mal^{2-} + H^+]^-$	133.01	133.01
	134.02	134.02
$[V^V_2O_5(mal)]^{2-}$	156.93	156.93
	157.44	157.44
	157.94	157.94
$[V^{IV}V^VO_5]^-$	181.86	181.86
$[HV^V_2O_6]^-$	198.87	198.87
$[V^VO_2(mal)]^-$	214.94	214.94
	215.94	215.94
$[V^V_3O_8]^-$	280.79	280.79
$[V^V_2O_4(mal) - H^+]^-$	296.87	296.87
	297.87	297.87
$[V^V_2O_5(mal)^{2-} + Cs^+]^-$	446.77	446.77
	447.78	447.78

with rmsd between carbon alpha atoms which is as low as 0.35 Å, and similar to that of the metal-free protein (rmsd = 0.24–0.27 Å).

Interestingly, the two structures differ in the V-containing fragments present in the crystal and in how these fragments interact with nearby protein residues.

In the structure solved using the lowest resolution data (structure **A**, Fig. 6A), coordination of a VO group, assigned to $[V^{IV}O]^{2+}$, to the side chain of Asp18 (Fig. S3†), non-covalent binding of the dinuclear oxidovanadium(V) complex $[V^V_2O_5(mal)]^{2-}$ to protein surface residues (Fig. 7A) and covalent binding of $[V^V_{10}O_{26}]^{2-}$ to the side chains of Glu7 and its symmetry mate (Glu7*) (Fig. 7B) are observed.

In the structure **A**, refinements suggest occupancy = 1.00, 0.70 and 0.70 for the $[V^{IV}O]^{2+}$, $[V^V_2O_5(mal)]^{2-}$ and $[V^V_{10}O_{26}]^{2-}$, respectively. $[V^{IV}O]^{2+}$ has not been detected in the ^{51}V NMR spectra of the compound but $[V^V_2O_5(mal)]^{2-}$ has been observed with ^{51}V NMR and mass spectrometry, while $[V^V_{10}O_{26}]^{2-}$ can be considered as a species derived by $[V^V_{10}O_{28}]^{6-}$ – observed in the NMR and ESI-MS spectra – with the two oxygen atoms from the protein. The $[V^{IV}O]^{2+}$ ion covalently bound to the OD1 atom of the Asp18 (Fig. S3†) is also in contact with the ND2 and OD1 atoms of Asn19, whose side chain adopts two different conformations. The dinuclear oxidovanadium(V) complex $[V^V_2O_5(mal)]^{2-}$ is the product of the loss of one mal ligand from $[V^V_2O_4(mal)_2]^{2-}$, *i.e.*, the species observed in the NMR spectra. The ligand loss can be explained by the behaviour of $[V^V_2O_4(mal)_2]^{2-}$ in an aqueous solution and could be favoured by the crystal packing and by the proximity of the dinuclear oxidovanadium(V) complex to the side chain of Asn65. The anion consists of two V centres both coordinated to two oxido ligands and two bridging oxygens, one of which is part of the mal ligand. One of the two V centres also binds an additional oxygen of the mal anion, forming a five-membered chelated ring (Fig. 8). Thus, in this structure the V centres are not equivalent. One V is penta-coordinate and the other is tetra-coordinated, at variance with what found in the structure of $Cs_2[V^V_2O_4(mal)_2]\cdot 2H_2O$, that is based on a centrosymmetric dimeric arrangement where the two metals show the same coordination spheres.[78] $[V^V_2O_5(mal)]^{2-}$ interacts with atoms and groups of the Gly67-Ser72 residues. In particular, the O^1 atom of $[V^V_2O_5(mal)]^{2-}$ is hydrogen bonded to the O of Thr69, N of Pro70 and a water molecule; O^4, O^6 and O^7 atoms of $[V^V_2O_5(mal)]^{2-}$ are hydrogen bonded to water molecules; O^5 forms hydrogen bonds with O atom of Gly67 and a water molecule; O^8 with O atom of Thr69, OG of Ser72 and water molecules; O^9 is hydrogen bonded to the N atom of Gly67, N of Arg68, N and O atoms of Thr69 and a water molecule and O^{10} with OD1 and ND2 of Asn65 and N of Gly67 (Fig. 7A).

The $[V^V_{10}O_{26}]^{2-}$ moiety present in the structure **A** is reconstituted by its symmetry mate and can be described as the decavanadate ion $[V^V_{10}O_{28}]^{6-}$ (ref. 84 and 85) that has two oxygens replaced by O atoms of the side chains of Glu7 and Glu7* (that adopt two alternative conformations with occupancy 0.70 and 0.30) (Fig. 7B). With this arrangement the decavanadate ion cross-links two protein molecules (Fig. S5†). $[V^V_{10}O_{26}]^{2-}$ forms hydrogen bonds with the NH2 atom of Arg14, the main chain O atom of Ser86, water molecules and NH2 atom of Arg14 from a symmetry-related molecule (Fig. 7B).

Although the interaction of decavanadate with proteins has been already studied by many groups using different techniques, including X-ray crystallography,[48] the formation of a covalent adduct between $[V^V_{10}O_{28}]^{6-}$ and a protein previously hypothesized[86] has never been confirmed structurally.

The Cambridge Crystallographic Data Centre (CCDC) contains over 300 distinct X-ray structures of decavanadate. In these structures, both the protonation state and the counter ions vary.[84] In the acidic pH range, decavanadate is a stable form (thermodynamic sink), while in the neutral pH range it is not stable but is kinetically inert and stays in solution for days.[84] Only two CCDC structures of decavanadate have two

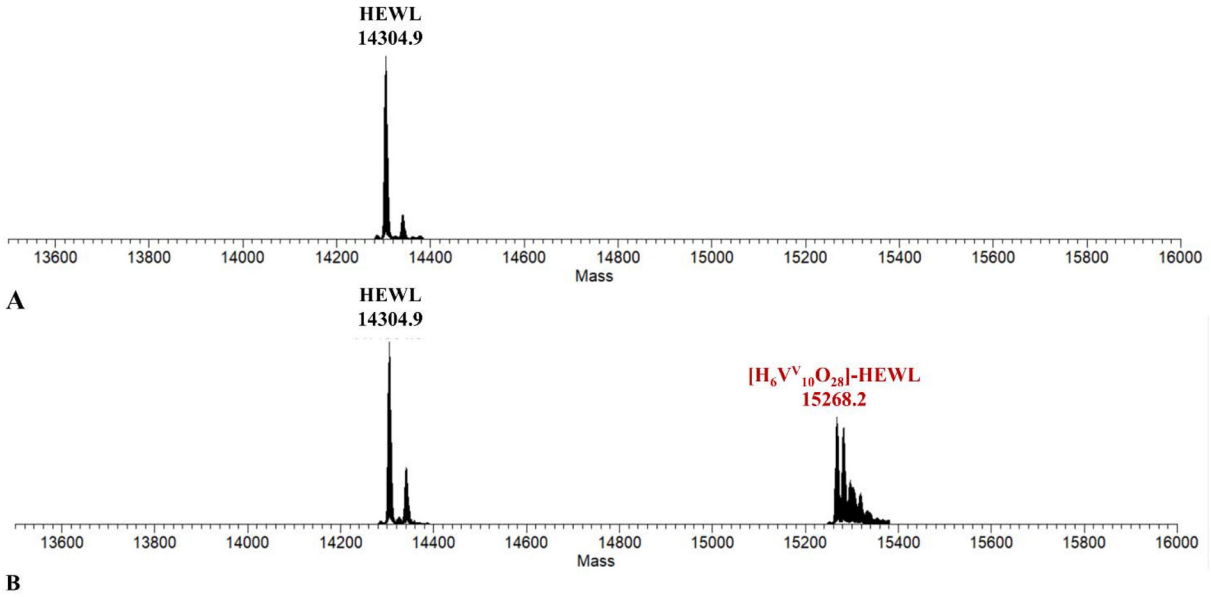

Fig. 5 Deconvoluted ESI-MS spectra of HEWL (concentration = 13 mg mL^{-1}) (A) and of the system containing $Cs_2[V^V_2O_4(mal)_2]\cdot 2H_2O$: HEWL in 1 : 1 molar ratio (B). Both samples were diluted 1 : 100 in acetonitrile/H_2O + 1% FA. Mass is in Da.

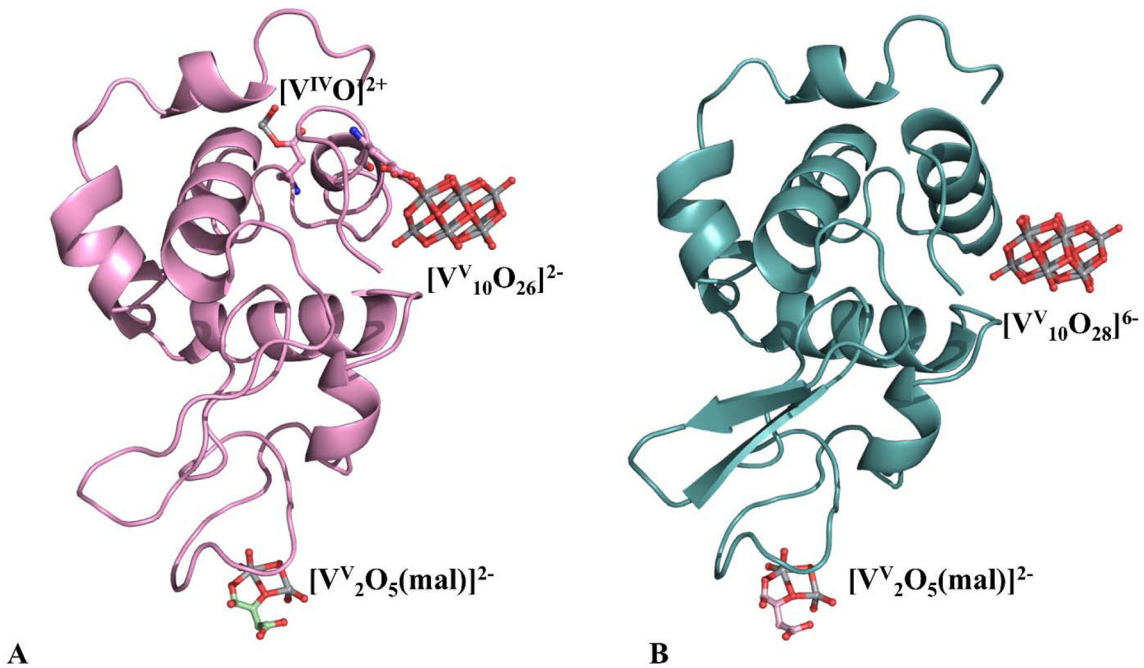

Fig. 6 Overall structures of V–HEWL adducts derived from two crystals of HEWL exposed to $Cs_2[V^V_2O_4(mal)_2]\cdot 2H_2O$ for 7 days: (A) Structure **A**; (B) structure **B**. Vanadium atoms are in grey. Coordinates and structure factors were deposited in the PDB under the accession codes 9RBG, and 9RBT.

oxygen atoms of the $\{V_{10}O_{28}\}$ core that are replaced by other groups: the structure deposited under the accession code HEGBEB[87] and that with code TORXAA.[88] In the former structure, two methoxy groups bridge the outermost V atoms;[87] in the latter two ethoxy groups bridge the outermost V atoms.[88] Notably, the CCDC does not contain decavanadate structures where two oxygens are replaced by two carboxylate groups, making our structure the first reported example of this substitution.

In the structure solved using the highest resolution data (structure **B**, Fig. 6B), non-covalent binding of both the dinuclear oxidovanadium(V) complex $[V^V_2O_5(mal)]^{2-}$ and $[V^V_{10}O_{28}]^{6-}$ is observed. $[V^V_{10}O_{28}]^{6-}$ is reconstructed by its symmetry mate, has occupancy equal to 0.80 and forms hydrogen bonds with

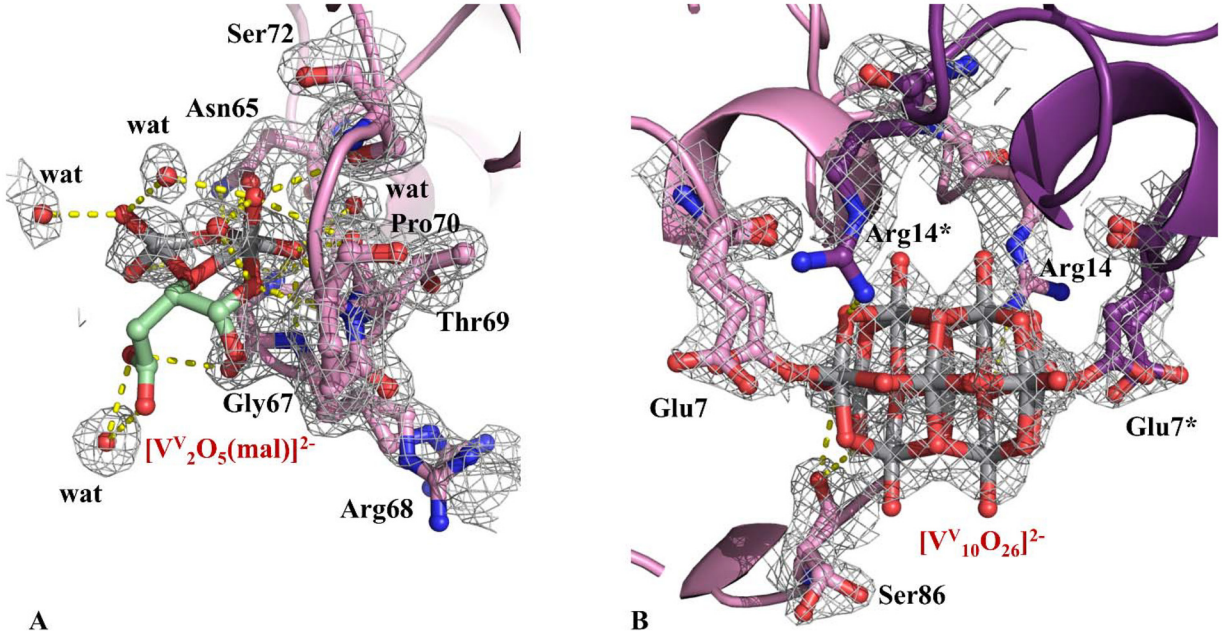

Fig. 7 Vanadium binding sites in the structure **A**: (A) non-covalent interaction of the dinuclear oxidovanadium(V) complex $[V^{V}_{2}O_5(mal)]^{2-}$ to the protein surface; (B) covalent binding of the $[V^{V}_{10}O_{26}]^{2-}$ to the side chain of Glu7 and Glu7*. 2Fo–Fc electron density maps are reported at 1.0σ level in grey. Anomalous difference electron density map is reported in Fig. S4A.† Asterisk refers to atoms from symmetry-related molecules (coloured in purple). Glu7 and Arg86 side chains adopt two alternative conformations.

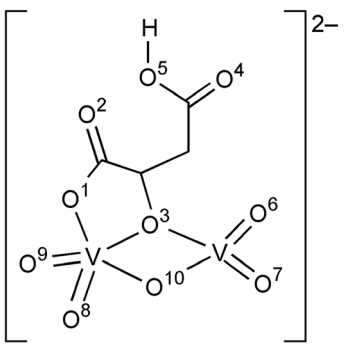

Fig. 8 Structure of $[V^{V}_{2}O_5(mal)]^{2-}$ complex.

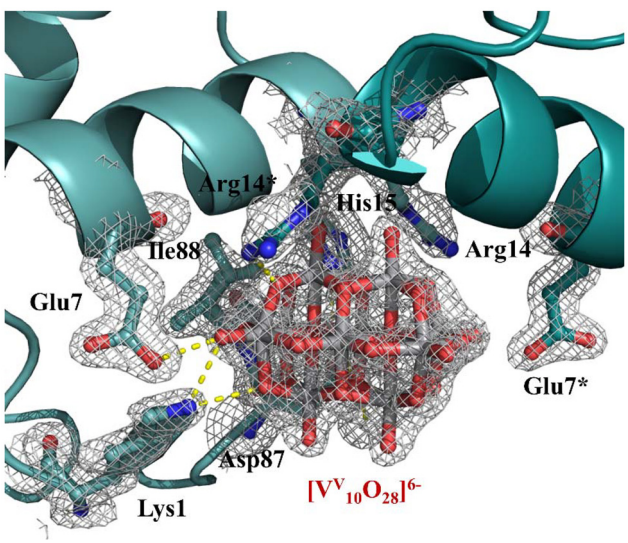

Fig. 9 Vanadium binding sites in structure **B**: non-covalent interaction of the $[V^{V}_{10}O_{28}]^{6-}$ to the protein surface. 2Fo–Fc electron density maps are reported at 1.0σ level in grey. Asterisk refers to atoms from symmetry-related molecules (deep teal). Anomalous difference electron density map is reported in Fig. S4B.†

the NZ atom of Lys1, OE2 atom of Glu7, NE2 of His15, OD2 of Asp87, the main chain N atom of Ile88, water molecules and the NH1 atom of Arg14 from a symmetry-related molecule (Fig. 9). These interactions are favoured by conformational variations of the side chains of Lys1, Glu7, Arg14 and His15 which change their conformation or their position when compared to the structure **A.**

The NMR, ESI-MS and crystallographic data can be discussed considering the behaviour of the systems formed by $V^{V}O_2^{+}$ ion and α-hydroxycarboxylates in aqueous solution. In the literature the stability constants of the complexes $V^{V}O_2$–mal are lacking but those of the species $V^{V}O_2$–citr, where citr is citrate anion,[80] can be useful to rationalize the experimental findings. Malic and citric acid are structurally similar (Fig. S6†), the difference being the fourth group bound to the tetrahedral central C, one H atom in the first case and one –CH_2COOH group in the second one (Fig. S6†). The fully protonated forms of malic and citric acid can be denoted with H_2L and H_3L and the pK_a values are comparable: pK_{a1} = 3.16 and pK_{a2} = 4.57 for malic acid,[89] and pK_{a1} = 2.87, pK_{a2} = 4.27 and

pK_{a3} = 5.57 for citric acid,[90] the difference being explained with the electron withdrawing effect of the third carboxylic group (C^3OOH in Fig. S6†). Therefore, a similar behaviour of the two ligands is expected, taking into account that the additional carboxylate group of citric acid is not coordinating. The distribution curve of the species formed by citrate and $V^VO_2^+$ ion with a molar ratio of 1 : 1 and a V concentration of 100 mM (ESI-MS experiments), 300 μM (soaking experiments) and 5 mM (NMR) can be calculated with the stability constants determined by Pettersson *et al.*[80] They are shown in Fig. S7.†

It can be observed that at pH 4.0, *i.e.*, the value used for the ESI-MS experiments, the species $[V^V_2O_5(Hcitr)]^{2-}$, with the (C^1OO^-, O^-) donor set bound to V^V and C^2OOH and C^3OOH groups still protonated, dominates in an aqueous solution; this species corresponds to $[V^V_2O_5(mal)]^{2-}$ where the coordination is (C^1OO^-, O^-) and C^2OOH is protonated. Based on these comments, in aqueous solution and around pH 4.0, the transformation of $[V^V_2O_4(mal)_2]^{2-}$ to $[V^V_2O_5(mal)]^{2-}$ occurs upon the reaction $[V^V_2O_4(mal)_2]^{2-} + H_2O \rightarrow [V^V_2O_5(mal)]^{2-} + H_2mal$. This explains the non-covalent binding of $[V^V_2O_5(mal)]^{2-}$ to HEWL, characterized by X-ray diffraction analysis (see Fig. 8) and the detection of this species in the ESI-MS and NMR experiments.

The analysis of Fig. S7† shows that, by increasing the V concentration, the amount of $[H_2V^V_2O_7]^{2-}$and $[HV^V_2O_7]^{3-}$ increases and polynuclear species such as $[V^V_4O_{12}]^{4-}$ and $[V^V_5O_{15}]^{5-}$ are formed. Notably, POVs with higher nuclearity are not expected, at least up to 5 mM, while V_{10} is detected both by ESI-MS and NMR. This finding could be explained by the greater stability of $[V^V_2O_5(Hcitr)]^{2-}$ than $[V^V_2O_5(mal)]^{2-}$ which could prevent the formation of decavanadate. Furthermore, it should be added that the amount of $[V^V_{10}O_{28}]^{6-}$ observed in the NMR experiments is small and its formation could be stabilized by the presence of HEWL at RT, as can be argued from Fig. 5, where the only adduct revealed by ESI-MS in the system formed by $Cs_2[V^V_2O_4(mal)_2]\cdot 2H_2O$ and protein is $[H_6V^V_{10}O_{28}]$–HEWL.

Finally, it should be noted that, once formed, a small amount of $[V^V_2O_5(mal)]^{2-}$ can give the aquaion $[V^VO_2]^+$ according to the reaction $[V^V_2O_5(mal)]^{2-} + 4H^+ \rightarrow 2\ [V^VO_2]^+ + H_2mal + H_2O$. Subsequently, $[V^VO_2]^+$ can be reduced to $[V^{IV}O]^{2+}$, which was detected in the structure **A** (Fig. 6A).

Interaction of HEWL with $Cs_2[V^V_2O_4(mal)_2]\cdot 2H_2O$: crystallographic studies at physiological temperature

Since ^{51}V NMR data suggest that at 37 °C in the presence of the protein V_{10} is not formed, we decided to study the structure of the V–HEWL adduct formed using a HEWL crystal grown at 37 °C and treated with $Cs_2[V^V_2O_4(mal)_2]\cdot 2H_2O$ at this temperature. Crystallization and data collection at 37 °C are challenging and require attention. A higher protein concentration was necessary to grow HEWL crystals at 37 °C, while special manipulations were needed for the crystal mounting on the goniometer, to avoid crystal dehydration. To collect X-ray diffraction data at 37 °C of HEWL crystals treated with $Cs_2[V^V_2O_4(mal)_2]\cdot 2H_2O$ (PDB code: 9RBV) we have used the procedure described in our previous work.[82] X-ray diffraction data have been collected at 37 °C at 2.09 Å resolution (Table S1†). The overall HEWL conformation in the 37 °C structure is not significantly affected by the temperature, in agreement with previous observation[82,91] (rmsd with metal-free protein structure = 0.20 Å and rmsd with the structure of the V–HEWL adducts reported in the previous paragraph = 0.27 Å and 0.35 Å). However, the structure reveals significant differences when compared to those described above at level of V-containing fragments that are bound to the protein. Indeed, in agreement with ^{51}V NMR spectra, in the 37 °C structure V_{10} is not observed, while a single VO group, presumably a $[V^{IV}O]^{2+}$ ion, is bound to the side chain of Asp18 (Fig. S8†).

Docking simulations

HEWL–$[V^V_2O_5(mal)]^{2-}$ adduct. The non-covalent docking of $[V^V_2O_5(mal)]^{2-}$ with HEWL resulted in six clusters, the first three having the highest *Fitness* score (F_{max} in the range 26.7–27.7) and including 80% of the solutions. All the found poses are located in the enzyme active site that is far from the observed binding pocket. In Fig. S9A† the cluster I is shown, where $[V^V_2O_5(mal)]^{2-}$ forms hydrogen bonds with the backbone NH of Asn59, NE1 of Trp63, and COOH groups of Asp52 (calculated value of pK_a with H++ software ~5.0). Clusters II and III (Fig. S9B and S9C†) show a hydrogen bond between COO^- of Glu35 and protonated COOH of the malate.

Since docking on a single HEWL chain does not reproduce the observed binding site, a "symmetry mate" docking approach was adopted. This strategy involves docking not only to one protein chain of HEWL, but also to the surrounding crystal lattice environment near the observed binding site of $[V^V_2O_5(mal)]^{2-}$. With this approach, the found solutions approximate the experimental structure (Fig. S10†). However, the best result is obtained if, in addition to the symmetry mates of HEWL, the symmetry mate of $[V^V_2O_5(mal)]^{2-}$, Na^+ ions, and crystallographic waters were considered. Two clusters, I and II (F_{max} values of 28.4 and 28.7, and population of 44% and 24%) were obtained, with cluster I well reproducing the crystallographic outcome (Fig. 10). Indeed, in the crystal lattice $[V^V_2O_5(mal)]^{2-}$ is located near one of its symmetry mates (Fig. S11A†) and Na^+ ions, hexa-coordinated by four protein donors and two water molecules (Fig. S11B†), contribute to form a hydrogen bond network which stabilizes the observed pose.

In the pose shown in Fig. 10, $[V^V_2O_5(mal)]^{2-}$ interacts directly with a protein chain through hydrogen bonds with Asn65, Gly67, Thr69 and Ser72, exactly as observed in the crystal structure. Moreover, the docking unveils that water molecules are engaged in a hydrogen bond network, bridging the HEWL symmetry mates to the dinuclear V^V complex and – through the two H_2O molecules highlighted in cyan in Fig. 10 – the two vanadium complexes.

HEWL–$[V^V_{10}O_{26}]^{2-}$ and HEWL–$[V^V_{10}O_{28}]^{6-}$ adducts. The crystallographic results show non-covalent interaction of $[V^V_{10}O_{28}]^{6-}$ and covalent interaction of $[V^V_{10}O_{26}]^{2-}$ with two adjacent symmetry mate HEWL chains in the crystal lattice. The molecular docking results confirm the binding of $[V^V_{10}O_{26}]^{2-}$

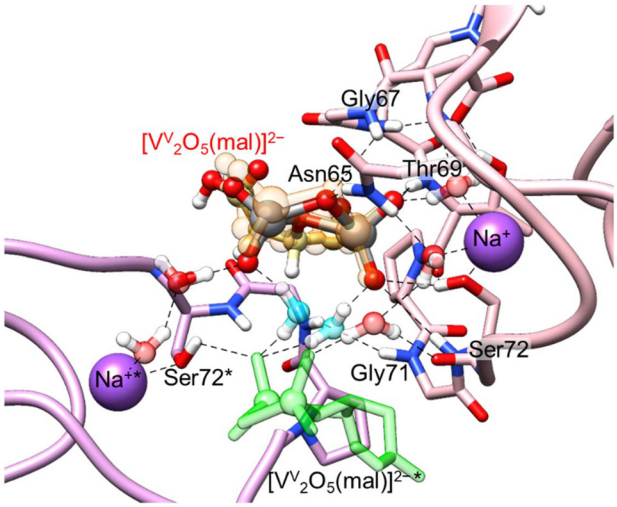

Fig. 10 Best docking pose of cluster I with non-covalent binding of $[V^{V}_{2}O_5(mal)]^{2-}$ at the symmetry mate-recreated site with crystallographic waters, Na^+ ions (purple spheres), and symmetry mate V^{V} complex (green). The asterisk indicates the residue of HEWL symmetry mate chains (different shades of pink/purple). Hydrogen bonds are indicated with dashed lines. For comparison, $[V^{V}_{2}O_5(mal)]^{2-}$ is reported in orange and in transparency with its crystallographic coordinates. The water molecules bridging the complex symmetry mates are highlighted in cyan.

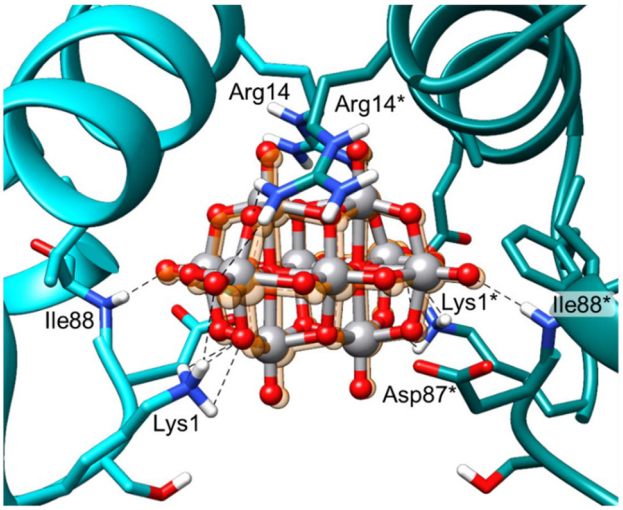

Fig. 11 Best docking pose of cluster I for the binding of $[V^{V}_{10}O_{28}]^{6-}$ between the two HEWL chains. The asterisks indicate the residues of the HEWL symmetry mate chain (deep teal). Hydrogen bonds are indicated with dashed lines. For comparison, $[V^{V}_{10}O_{28}]^{6-}$ is reported in transparent orange with its crystallographic coordinates.

and $[V^{V}_{10}O_{28}]^{6-}$ at the interface between the two HEWL chains, exactly as they are arranged in the crystal.

The non-covalent binding of $[V^{V}_{10}O_{28}]^{6-}$ can be reproduced only by the "symmetry mate" approach. This suggests that the protein–protein interaction can play a fundamental role in the stabilization of the adducts formed by a V species (and, in general, by a metal species). The results show that $[V^{V}_{10}O_{28}]^{6-}$ interacts with the residues Lys1, Arg14, and Ile88 of both HEWL chains. The docking solutions were grouped in four clusters (I–IV) through rmsd analysis and ranked on the basis of *F* values. Cluster I shows the best *F* value (27.0) and higher population (83%) and is in very good agreement with the crystallographic result (Fig. 11). The clusters II–IV share the remaining 17% of the solutions and consist of poses of $[V^{V}_{10}O_{28}]^{6-}$ with different orientations when compared to cluster I, but interacting with the same protein residues.

To study the covalent docking of $[V^{V}_{10}O_{26}]^{2-}$, two oxygen atoms of the anion were replaced by two dummy hydrogens. The experimental crystallographic results are reproduced only when Lys1, Glu7, and Arg14 side chains are free to move. With this approach, eighteen clusters of solutions (I–XVIII) were obtained; among them, seven clusters (I, II, III, IV, VI, VIII, and IX) present covalent bonds with Glu7 and Glu7* and various orientation of the polyoxido anion compared with the experimental data. Cluster I has highest *F* score and optimizes the interaction with the residues Lys1, Arg14, and Ile88 (Fig. 12); cluster IX, despite having the lowest *F* value, best resembles the crystallographic outcome (Fig. S12†).

Six clusters (V, VII, X, XI, XIII, and XV) exhibit an alternative solution, based on the covalent bonds with Asp87 and Asp87* residues (Fig. S13A†), while clusters XII and XIV show a mixed situation, namely a covalent bond with Glu7 of a HEWL chain and a covalent bond with Asp87* (Fig. S13B†). Notably, the covalent interaction of Asp87 and Asp87*, located close to Glu7 and Glu7* in the space between the two proteins, was recently assessed for $[V_{20}O_{54}(NO_3)]^{n-}$ and $[V_{20}O_{51}(OH_2)]^{n-}$

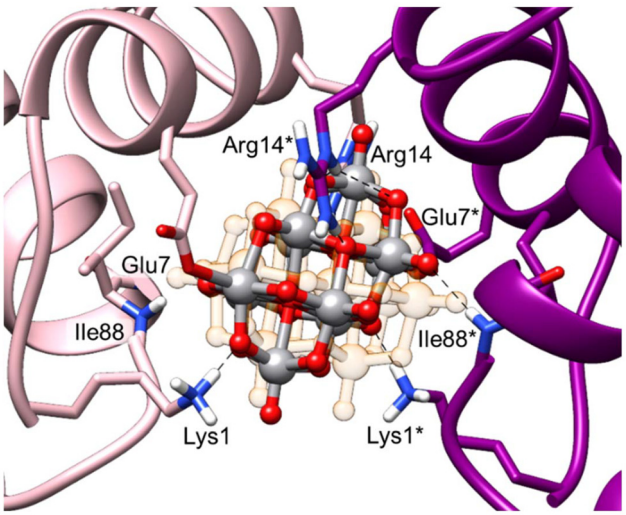

Fig. 12 Best covalent docking pose of cluster I of $[V^{V}_{10}O_{26}]^{2-}$ between the two HEWL chains. The asterisks indicate the residues of the HEWL symmetry mate chain (purple). Hydrogen bonds are indicated with dashed lines. For comparison, a transparent orange $[V^{V}_{10}O_{26}]^{2-}$ is reported in orange and in transparency with its crystallographic coordinates.

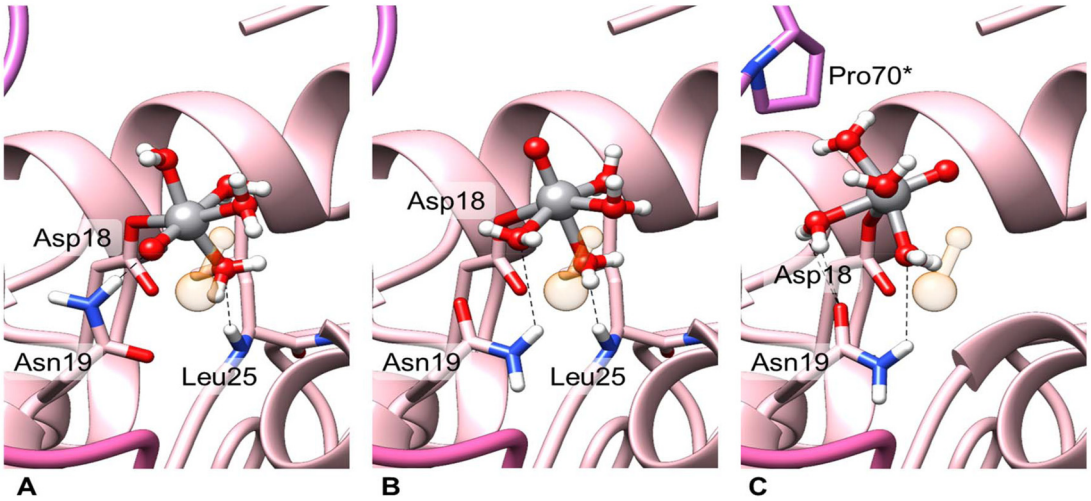

Fig. 13 Best covalent docking poses of $[V^{IV}O]^{2+}$ at the symmetry mate-recreated binding site: (A) cluster I; (B) cluster II; (C) cluster III. The asterisk indicates the residue of HEWL symmetry mate chains (different shades of pink/purple). Hydrogen bonds are indicated with dashed lines. For comparison, the experimentally revealed VO group is reported in orange and in transparency with its crystallographic coordinates.

anions.[38,43,82] The pK_a values of Glu7 and Asp87 calculated with H^{++} are ~0.8 and <0, respectively, suggesting that both are 100% deprotonated at pH 4.0 and thus can coordinate V^V centres. This indicates that this site offers more covalent binding possibilities to $[V^V_{10}O_{26}]^{2-}$ between the HEWL chains and, more in general, it favours the covalent as well as non-covalent binding of POVs. The binding with the accessible residues depends on the specific POV between the two chains which determines the type and strength of the interaction.

Finally, the clusters with lowest *F* scores (XVI, XVII, and XVIII) present poses with only one covalent bond with Glu7 (XVI) or with none (XVII and XVIII). From a kinetic point of view, it cannot be ruled out that this solution might represent an intermediate situation, before the most stable pose with covalent bonds to Glu7 and Glu7*. In other words, we can imagine initially the binding of Glu7, followed by Asp87* (cluster XII and XIV, see above); then, upon the cleavage of the latter, the polyoxidovanadate migrates toward the central part of the pocket between the chains, where stable non-covalent interactions with Lys1, Arg14, and His15 are established and covalent bond with Glu7* is formed. This is graphically represented in Fig. S14.†

HEWL–$[V^{IV}O]^{2+}$ adduct. For the covalent molecular docking of $[V^{IV}O]^{2+}$, the hexa-coordinated $[V^{IV}O(H_2O)_5]^{2+}$ aquaion was considered. To simulate the coordination by the protein during docking, one of the aqua ligands in *cis* to the oxido ligand was substituted by a dummy hydrogen atom. The docking results using a single HEWL chain show two different binding sites but do not reproduce the crystallographic findings. The solutions are grouped into four clusters: cluster I, with highest *F*, presents a covalent bond with the nitrogen atom NE2 of His15 (Fig. S15A†), while clusters II–IV correspond to the binding site in the enzymatic pocket of HEWL and show V–O bond with Asp52 (II and IV, Fig. S15B) and Glu35 (III, Fig. S15C†). The covalent binding to HEWL by Asp52 was demonstrated by X-ray crystallography for $[V^{IV}O(pic)_2]$, $[V^{IV}OCl(H_2O)_2]^+$, $[V^{IV}O(bipy)]^{2+}$, and $[V^{IV}O(phen)]^{2+}$ moieties,[49,92] while with Glu35 by X-ray and docking for $[V^{IV}O(H_2O)_3]^{2+}$ and $[V^{IV}O(malt)_2]$,[35,39] where pic, bipy, phen, malt stand for picolinato, 2,2′-bipyridine, 1,10-phenanthroline, maltolato ligands, respectively; these results indicate that this is one of the favoured sites for V–HEWL interaction. The fact that these sites were not experimentally revealed in this study could depend on pH used to crystallize the adducts. Indeed, at pH 4.0, His15 is surely protonated, while for Asp52 and Glu35 H^{++} software predicts pK_a ~ 5.0 (90% protonated) and ~4.0 (50% protonated), respectively. Notably, the experimental data can be reproduced if the simulations are performed by recreating the environment around the observed binding site in the crystal lattice, using the "symmetry mate" approach (Fig. S16†). The solutions are grouped in three similar clusters, each of them consisting of only one pose: a coordinative bond between the V^{IV} centre and Asp18 is formed, along with hydrogen bonds between Asn19 and the oxido and/or the aqua ligands (Fig. 13). Interestingly, the calculated pK_a of carboxylic group of Asp18 is ~2.1, significantly lower than Glu35 and Asp52, meaning that it is ~100% deprotonated.

Conclusions

In conclusion, here we have studied the solution behaviour of $Cs_2[V^V_2O_4(mal)_2]\cdot 2H_2O$, a VC containing the active bioligand malato and belonging to the family of α-hydroxycarboxylates, under various experimental conditions and in the absence and in the presence of HEWL. $Cs_2[V^V_2O_4(mal)_2]\cdot 2H_2O$, like many other VCs, is unstable in aqueous solution and – depending on pH and V concentration – can undergo transformation into

a variety of V-containing species which can interact with proteins through multiple binding modes and stabilization mechanisms.[38,43,81,82]

According to ^{51}V NMR spectroscopic investigations and mass spectrometry data, at RT, the dinuclear V^V compound forms species with two and ten V (V_{10}) centres, both in the absence and presence of the protein. At physiological temperature the percentage of decavanadate increases over time in the absence of HEWL, while it decreases over time and completely disappears after 7 days in the presence of the protein. To analyse in detail the interactions that the V-containing species – produced in solution from $[V^V_2O_4(mal)_2]^{2-}$ – are able to form with HEWL, X-ray structures of the protein in the presence of the V compound have been solved. Two different crystals at cryogenic temperature and an additional crystal of HEWL grown at 37 °C, on which X-ray diffraction data have been collected at physiological temperature, have been analysed. Results reveal that, in *crystallo*, HEWL binds a $[V^{IV}O]^{2+}$ ion, a $[V^V_2O_5(mal)]^{2-}$ ion and a V_{10} group at 20 °C, while at physiological temperature the decavanadate disappears, in strict agreement with ^{51}V NMR data, and only an adduct with $[V^{IV}O]^{2+}$ ion is observed. We report the first structural observation of non-covalent and covalent interaction of V_{10} to a protein, the covalent binding being formed upon replacement of two O atoms of $[V^V_{10}O_{28}]^{6-}$ by carboxylate groups from Glu7 and Glu7*. The formation of the adducts with $[V^V_2O_5(mal)]^{2-}$, $[V^V_{10}O_{26}]^{2-}$ and $[V^V_{10}O_{28}]^{6-}$ is favoured by protein–protein interaction, as confirmed by docking calculations.

As recently reviewed in the literature,[57] this may have important implications in the transport mechanism and mode of action of V-based drugs. Regarding the results of this study, in some cases the V complex transformation can be explained with the behaviour expected in aqueous solution at pH 4.0 on the basis of the thermodynamic stability constants; in other cases, instead, for example in the case of V_{10}, the transformation cannot be easily predicted. In this respect, it should be noted that the binding of V-containing fragments can be covalent and non-covalent and protein–protein interaction, established by X-ray diffraction analysis and docking calculations, can stabilize the adducts. As pointed out in a recent study,[44] whether protein–protein stabilization contributes to metal–protein interaction in solution remains uncertain even if some experimental result in the literature suggested that this might be possible in some systems, for example between HEWL and oxaliplatin.[93] In any case, it is well established that protein–protein interactions occur in solution,[94–96] so it does not seem unlikely – as noted by several authors[97] – that crystal contacts can reflect biologically relevant interactions. Overall, our findings suggest that protein–protein stabilization may facilitate unexpected binding events between metal-containing fragments and proteins, as already suggested by other groups.[98] Here, we would like to highlight that this phenomenon might be more widespread than previously recognized and should be considered in the interpretation of the behaviour of systems containing a metal-based drug and a physiologically relevant protein.

Author contributions

M. P.: data curation, writing – original draft, investigation. G. F.: data curation, investigation. N. I. G.: data curation, investigation, funding acquisition, supervision, writing – review & editing. F. P.: data curation, writing – original draft, investigation. E. G.: conceptualization, funding acquisition, supervision, writing – review & editing. A. R.: conceptualization, funding acquisition, supervision, writing – review & editing. A. M.: conceptualization, funding acquisition, supervision, writing – review & editing.

Conflicts of interest

The authors have no conflict of interest to declare.

Data availability

Data are all available in literature or deposited in the PBD.

Acknowledgements

This research was funded by MIUR PRIN 2022 – Cod. 2022JMFC3X "Protein Metalation by Anticancer Metal-based Drugs", MIUR PRIN 2022 – Cod. 2022APCTNA "TRILLI – TRansforming metal Ions and Low-cost LIgands into next generation metallodrugs. A thermodynamic, spectroscopic and biological approach for their rational design" and in part by the Austrian Science Fund (FWF) [**https://doi.org/10.55776/P33089** (to A. R.); **https://doi.org/10.55776/P33927** (to N. G.)]. Financial support from the University of Vienna is acknowledged. For open access purposes, the author has applied a CC BY public copyright license to any author who accepted manuscript version arising from this submission.

References

1 J. Costa Pessoa, S. Etcheverry and D. Gambino, Vanadium compounds in medicine, *Coord. Chem. Rev.*, 2015, **301–302**, 24–48.
2 E. Kioseoglou, S. Petanidis, C. Gabriel and A. Salifoglou, The chemistry and biology of vanadium compounds in cancer therapeutics, *Coord. Chem. Rev.*, 2015, **301–302**, 87–105.
3 A. Ścibior, J. Llopis, A. A. Holder and M. Altamirano-Lozano, Vanadium Toxicological Potential versus Its Pharmacological Activity: New Developments and Research, *Oxid. Med. Cell. Longevity*, 2016, **2016**, 7612347.
4 D. Rehder, Perspectives for Vanadium in Health Issues, *Future Med. Chem.*, 2016, **8**, 325–338.
5 D. C. Crans, L. Henry, G. Cardiff and B. I. Posner, *Developing Vanadium as an Antidiabetic or Anticancer Drug: A*

Clinical and Historical Perspective, ed. P. L. Carver, De Gruyter, Berlin, 2019, pp. 203–230..
6 S. Treviño, A. Díaz, E. Sánchez-Lara, B. L. Sanchez-Gaytan, J. M. Perez-Aguilar and E. González-Vergara, Vanadium in Biological Action: Chemical, Pharmacological Aspects, and Metabolic Implications in Diabetes Mellitus, *Biol. Trace Elem. Res.*, 2019, **188**, 68–98.
7 D. Rehder, The potentiality of vanadium in medicinal applications, *Inorg. Chim. Acta*, 2020, **504**, 119445.
8 C. Amante, A. L. De Sousa-Coelho and M. Aureliano, Vanadium and Melanoma: A Systematic Review, *Metals*, 2021, **11**, 828.
9 M. Aureliano, N. I. Gumerova, G. Sciortino, E. Garribba, A. Rompel and D. C. Crans, Polyoxovanadates with emerging biomedical activities, *Coord. Chem. Rev.*, 2021, **447**, 214143.
10 D. Sanna and E. Garribba, Pharmacologically Active Vanadium Species: Distribution in Biological Media and Interaction with Molecular Targets, *Curr. Med. Chem.*, 2021, **28**, 7339–7384.
11 A. A. Sharfalddin, I. M. Al-Younis, H. A. Mohammed, M. Dhahri, F. Mouffouk, H. Abu Ali, Md. J. Anwar, K. A. Qureshi, M. A. Hussien, M. Alghrably, M. Jaremko, N. Alasmael, J. I. Lachowicz and A.-H. Emwas, Therapeutic Properties of Vanadium Complexes, *Inorganics*, 2022, **10**, 244.
12 S. Semiz, Vanadium as potential therapeutic agent for COVID-19: A focus on its antiviral, antiinflamatory, and antihyperglycemic effects, *J. Trace Elem. Med. Biol.*, 2022, **69**, 126887.
13 L. M. P. F. Amaral, T. Moniz, A. M. N. Silva and M. Rangel, Vanadium Compounds with Antidiabetic Potential, *Int. J. Mol. Sci.*, 2023, **24**, 15675.
14 D. Rehder, Vanadium in biological systems and medicinal applications, *Inorg. Chim. Acta*, 2023, **549**, 121387.
15 A. P. Singh, S. Roy and I. C. Maurya, Vanadium complexes: potential candidates for therapeutic applications, *Transition Met. Chem.*, 2024, **49**, 101–119.
16 A. K. Renfrew, Transition metal complexes with bioactive ligands: mechanisms for selective ligand release and applications for drug delivery, *Metallomics*, 2014, **6**, 1324–1335.
17 L. H. Beatriz, A. Ángel, E.-B. Ana and H. Sonsoles, Metal-Based Compounds as Promising Anticancer Agents: An Overview on the Recent Literature, *Anti-Cancer Agents Med. Chem.*, 2019, **19**, 48–66.
18 F. Zechel, P. Schwendt, R. Gyepes, J. Šimunek, J. Tatiersky and L. Krivosudský, Vanadium(V) complexes of mandelic acid, *New J. Chem.*, 2019, **43**, 17696–17702.
19 E. Bermejo, R. Carballo, A. Castiñeiras and A. B. Lago, Coordination of α-hydroxycarboxylic acids with first-row transition ions, *Coord. Chem. Rev.*, 2013, **257**, 2639–2651.
20 P. Schwendt, J. Tatiersky, L. Krivosudský and M. Šimuneková, Peroxido complexes of vanadium, *Coord. Chem. Rev.*, 2016, **318**, 135–157.
21 A. S. Tracey, M. J. Gresser and K. M. Parkinson, Vanadium (V) Oxyanions. Interactions of Vanadate with Oxalate, Lactate, and Glycerate, *Inorg. Chem.*, 1987, **26**, 629–638.
22 S. Hati, R. J. Batchelor, F. W. B. Einstein and A. S. Tracey, Vanadium(V) Complexes of α-Hydroxycarboxylic Acids in Aqueous Solution, *Inorg. Chem.*, 2001, **40**, 6258–6265.
23 M. Tsaramyrsi, D. Kavousanaki, C. P. Raptopoulou, A. Terzis and A. Salifoglou, Systematic synthesis, structural characterization, and reactivity studies of vanadium(V)–citrate anions $[VO_2(C_6H_6O_7)]_2^{2-}$, isolated from aqueous solutions in the presence of different cations, *Inorg. Chim. Acta*, 2001, **320**, 47–59.
24 J. Omini, T. Dele-Osibanjo, H. Kim, J. Zhang and T. Obata, Is the TCA cycle malate dehydrogenase-citrate synthase metabolon an illusion?, *Essays Biochem.*, 2024, **68**, 99–106.
25 A. Kövilein, C. Kubisch, L. Cai and K. Ochsenreither, Malic acid production from renewables: a review, *J. Chem. Technol. Biotechnol.*, 2020, **95**, 513–526.
26 Z. Zhang, B. Wang, P. Zhou, D. Guo, R. Kang and B. Zhang, A novel approach of chemical mechanical polishing using environment-friendly slurry for mercury cadmium telluride semiconductors, *Sci. Rep.*, 2016, **6**, 22466.
27 C. L. Yiin, A. T. Quitain, S. Yusup, M. Sasaki, Y. Uemura and T. Kida, Characterization of natural low transition temperature mixtures (LTTMs): Green solvents for biomass delignification, *Bioresour. Technol.*, 2016, **199**, 258–264.
28 K. Radošević, N. Ćurko, V. Gaurina Srček, M. Cvjetko Bubalo, M. Tomašević, K. Kovačević Ganić and I. Radojčić Redovniković, Natural deep eutectic solvents as beneficial extractants for enhancement of plant extracts bioactivity, *LWT–Food Sci. Technol.*, 2016, **73**, 45–51.
29 V. Ugone, D. Sanna, G. Sciortino, D. C. Crans and E. Garribba, ESI-MS Study of the Interaction of Potential Oxidovanadium(IV) Drugs and Amavadin with Model Proteins, *Inorg. Chem.*, 2020, **59**, 9739–9755.
30 G. Sciortino, V. Ugone, D. Sanna, G. Lubinu, S. Ruggiu, J.-D. Maréchal and E. Garribba, Biospeciation of Potential Vanadium Drugs of Acetylacetonate in the Presence of Proteins, *Front. Chem.*, 2020, **8**, 345.
31 D. Biswal, N. R. Pramanik, S. Chakrabarti, M. G. B. Drew, K. Acharya and S. Chandra, Syntheses, crystal structures, DFT calculations, protein interaction and anticancer activities of water soluble dipicolinic acid-imidazole based oxidovanadium(IV) complexes, *Dalton Trans.*, 2017, **46**, 16682–16702.
32 J. Costa Pessoa, E. Garribba, M. F. A. Santos and T. Santos-Silva, Vanadium and proteins: Uptake, transport, structure, activity and function, *Coord. Chem. Rev.*, 2015, **301–302**, 49–86.
33 G. Sciortino, J.-D. Maréchal and E. Garribba, Integrated experimental/computational approaches to characterize the systems formed by vanadium with proteins and enzymes, *Inorg. Chem. Front.*, 2021, **8**, 1951–1974.
34 J. Costa Pessoa, M. F. A. Santos, I. Correia, D. Sanna, G. Sciortino and E. Garribba, Binding of vanadium ions and complexes to proteins and enzymes in aqueous solution, *Coord. Chem. Rev.*, 2021, **449**, 214192.
35 G. Ferraro, M. Paolillo, G. Sciortino, E. Garribba and A. Merlino, Multiple and Variable Binding of

Pharmacologically Active Bis(maltolato)oxidovanadium(IV) to Lysozyme, *Inorg. Chem.*, 2022, **61**, 16458–16467.

36 G. Ferraro, L. Vitale, G. Sciortino, F. Pisanu, E. Garribba and A. Merlino, Interaction of $V^{IV}O$–8-hydroxyquinoline species with RNase A: the effect of metal ligands in the protein adduct stabilization, *Inorg. Chem. Front.*, 2023, **10**, 5186–5198.

37 G. Ferraro, M. Paolillo, G. Sciortino, F. Pisanu, E. Garribba and A. Merlino, Implications of Protein Interaction in the Speciation of Potential $V^{IV}O$–Pyridinone Drugs, *Inorg. Chem.*, 2023, **62**, 8407–8417.

38 G. Ferraro, G. Tito, G. Sciortino, E. Garribba and A. Merlino, Stabilization and Binding of $[V_4O_{12}]^{4-}$ and Unprecedented $[V_{20}O_{54}(NO_3)]^{n-}$ to Lysozyme upon Loss of Ligands and Oxidation of the Potential Drug $V^{IV}O$(acetylacetonato)$_2$, *Angew. Chem.*, 2023, **135**, e202310655.

39 G. Sciortino, D. Sanna, V. Ugone, G. Micera, A. Lledós, J.-D. Maréchal and E. Garribba, Elucidation of Binding Site and Chiral Specificity of Oxidovanadium Drugs with Lysozyme through Theoretical Calculations, *Inorg. Chem.*, 2017, **56**, 12938–12951.

40 G. Sciortino, D. Sanna, V. Ugone, J.-D. Maréchal and E. Garribba, Integrated ESI-MS/EPR/computational characterization of the binding of metal species to proteins: vanadium drug–myoglobin application, *Inorg. Chem. Front.*, 2019, **6**, 1561–1578.

41 G. Sciortino, D. Sanna, V. Ugone, J.-D. Maréchal, M. Alemany-Chavarria and E. Garribba, Effect of secondary interactions, steric hindrance and electric charge on the interaction of $V^{IV}O$ species with proteins, *New J. Chem.*, 2019, **43**, 17647–17660.

42 V. Ugone, D. Sanna, G. Sciortino, J.-D. Maréchal and E. Garribba, Interaction of Vanadium(IV) Species with Ubiquitin: A Combined Instrumental and Computational Approach, *Inorg. Chem.*, 2019, **58**, 8064–8078.

43 G. Tito, G. Ferraro, F. Pisanu, E. Garribba and A. Merlino, Non–Covalent and Covalent Binding of New Mixed–Valence Cage–like Polyoxidovanadate Clusters to Lysozyme, *Angew. Chem., Int. Ed.*, 2024, **63**, e202406669.

44 M. Paolillo, G. Ferraro, F. Pisanu, J. Maréchal, G. Sciortino, E. Garribba and A. Merlino, Protein–Protein Stabilization in $V^{IV}O$/8–Hydroxyquinoline–Lysozyme Adducts, *Chem. – Eur. J.*, 2024, e202401712.

45 M. Paolillo, G. Ferraro, I. Cipollone, E. Garribba, M. Monti and A. Merlino, Unexpected *in crystallo* reactivity of the potential drug bis(maltolato)oxidovanadium(IV) with lysozyme, *Inorg. Chem. Front.*, 2024, **11**, 6307–6315.

46 M. Paolillo, G. Ferraro, G. Sahu, P. D. Pattanayak, E. Garribba, S. Halder, R. Ghosh, B. Mondal, P. B. Chatterjee, R. Dinda and A. Merlino, Interaction of $V^{V}O_2$–hydrazonates with lysozyme, *J. Inorg. Biochem.*, 2025, **264**, 112787.

47 D. Sanna, V. Ugone, G. Sciortino, P. Buglyó, Z. Bihari, P. L. Parajdi-Losonczi and E. Garribba, $V^{IV}O$ complexes with antibacterial quinolone ligands and their interaction with serum proteins, *Dalton Trans.*, 2018, **47**, 2164–2182.

48 M. Aureliano, N. I. Gumerova, G. Sciortino, E. Garribba, C. C. McLauchlan, A. Rompel and D. C. Crans, Polyoxidovanadates' interactions with proteins: An overview, *Coord. Chem. Rev.*, 2022, **454**, 214344.

49 M. F. A. Santos, G. Sciortino, I. Correia, A. C. P. Fernandes, T. Santos-Silva, F. Pisanu, E. Garribba and J. Costa Pessoa, Binding of $V^{IV}O^{2+}$, $V^{IV}OL$, $V^{IV}OL_2$ and $V^{V}O_2L$ Moieties to Proteins: X–ray/Theoretical Characterization and Biological Implications, *Chem. – Eur. J.*, 2022, **28**, e202200105.

50 G. Ferraro, N. Demitri, L. Vitale, G. Sciortino, D. Sanna, V. Ugone, E. Garribba and A. Merlino, Spectroscopic/Computational Characterization and the X-ray Structure of the Adduct of the $V^{IV}O$–Picolinato Complex with RNase A, *Inorg. Chem.*, 2021, **60**, 19098–19109.

51 S. Lima, A. Banerjee, G. Sahu, S. A. Patra, K. Sahu, T. Sasamori, G. Sciortino, E. Garribba and R. Dinda, New mixed ligand oxidovanadium(IV) complexes: Solution behavior, protein interaction and cytotoxicity, *J. Inorg. Biochem.*, 2022, **233**, 111853.

52 V. Ugone, D. Sanna, S. Ruggiu, G. Sciortino and E. Garribba, Covalent and non-covalent binding in vanadium–protein adducts, *Inorg. Chem. Front.*, 2021, **8**, 1189–1196.

53 A. Banerjee, S. P. Dash, M. Mohanty, G. Sahu, G. Sciortino, E. Garribba, M. F. N. N. Carvalho, F. Marques, J. Costa Pessoa, W. Kaminsky, K. Brzezinski and R. Dinda, New V^{IV}, $V^{IV}O$, $V^{V}O$, and $V^{V}O_2$ Systems: Exploring their Interconversion in Solution, Protein Interactions, and Cytotoxicity, *Inorg. Chem.*, 2020, **59**, 14042–14057.

54 G. Sciortino, D. Sanna, V. Ugone, A. Lledós, J.-D. Maréchal and E. Garribba, Decoding Surface Interaction of $V^{IV}O$ Metallodrug Candidates with Lysozyme, *Inorg. Chem.*, 2018, **57**, 4456–4469.

55 C. C. McLauchlan, B. J. Peters, G. R. Willsky and D. C. Crans, Vanadium–phosphatase complexes: Phosphatase inhibitors favor the trigonal bipyramidal transition state geometries, *Coord. Chem. Rev.*, 2015, **301–302**, 163–199.

56 M. F. A. Santos and J. Costa Pessoa, Interaction of Vanadium Complexes with Proteins: Revisiting the Reported Structures in the Protein Data Bank (PDB) since 2015, *Molecules*, 2023, **28**, 6538.

57 R. Dinda, E. Garribba, D. Sanna, D. C. Crans and J. Costa Pessoa, Hydrolysis, Ligand Exchange, and Redox Properties of Vanadium Compounds: Implications of Solution Transformation on Biological, Therapeutic, and Environmental Applications, *Chem. Rev.*, 2025, **125**, 1468–1603.

58 N. I. Gumerova and A. Rompel, Polyoxometalates in solution: speciation under spotlight, *Chem. Soc. Rev.*, 2020, **49**, 7568–7601.

59 N. I. Gumerova and A. Rompel, Speciation atlas of polyoxometalates in aqueous solutions, *Sci. Adv.*, 2023, **9**, eadi0814.

60 N. I. Gumerova and A. Rompel, Interweaving Disciplines to Advance Chemistry: Applying Polyoxometalates in Biology, *Inorg. Chem.*, 2021, **60**, 6109–6114.

61 A. Levina and P. A. Lay, Vanadium(V/IV)–Transferrin Binding Disrupts the Transferrin Cycle and Reduces Vanadium Uptake and Antiproliferative Activity in Human Lung Cancer Cells, *Inorg. Chem.*, 2020, **59**, 16143–16153.

62 E. Griffin, A. Levina and P. A. Lay, Vanadium(V) tris-3,5-di-tert-butylcatecholato complex: Links between speciation and anti-proliferative activity in human pancreatic cancer cells, *J. Inorg. Biochem.*, 2019, **201**, 110815.

63 C. Vonrhein, C. Flensburg, P. Keller, A. Sharff, O. Smart, W. Paciorek, T. Womack and G. Bricogne, Data processing and analysis with the *autoPROC* toolbox, *Acta Crystallogr., Sect. D:Biol. Crystallogr.*, 2011, **67**, 293–302.

64 A. J. McCoy, R. W. Grosse-Kunstleve, P. D. Adams, M. D. Winn, L. C. Storoni and R. J. Read, Phaser crystallographic software, *J. Appl. Crystallogr.*, 2007, **40**, 658–674.

65 M. C. Vaney, S. Maignan, M. Riès-Kautt and A. Ducruix, High-Resolution Structure (1.33 Å) of a HEW Lysozyme Tetragonal Crystal Grown in the APCF Apparatus. Data and Structural Comparison with a Crystal Grown under Microgravity from SpaceHab-01 Mission, *Acta Crystallogr., Sect. D:Biol. Crystallogr.*, 1996, **52**, 505–517.

66 G. N. Murshudov, A. A. Vagin and E. J. Dodson, Refinement of Macromolecular Structures by the Maximum-Likelihood Method, *Acta Crystallogr., Sect. D: Biol. Crystallogr.*, 1997, **53**, 240–255.

67 P. Emsley and K. Cowtan, *Coot* : model-building tools for molecular graphics, *Acta Crystallogr., Sect. D:Biol. Crystallogr.*, 2004, **60**, 2126–2132.

68 G. Jones, P. Willett, R. C. Glen, A. R. Leach and R. Taylor, Development and validation of a genetic algorithm for flexible docking, *J. Mol. Biol.*, 1997, **267**, 727–748.

69 R. Diamond, Real-space refinement of the structure of hen egg-white lysozyme, *J. Mol. Biol.*, 1974, **82**, 371–391.

70 G. Sciortino, J. Rodríguez-Guerra Pedregal, A. Lledós, E. Garribba and J. Maréchal, Prediction of the interaction of metallic moieties with proteins: An update for protein–ligand docking techniques, *J. Comput. Chem.*, 2018, **39**, 42–51.

71 G. Sciortino, E. Garribba and J.-D. Maréchal, Validation and Applications of Protein–Ligand Docking Approaches Improved for Metalloligands with Multiple Vacant Sites, *Inorg. Chem.*, 2019, **58**, 294–306.

72 J. C. Gordon, J. B. Myers, T. Folta, V. Shoja, L. S. Heath and A. Onufriev, H++: a server for estimating pKas and adding missing hydrogens to macromolecules, *Nucleic Acids Res.*, 2005, **33**, W368–W371.

73 E. F. Pettersen, T. D. Goddard, C. C. Huang, G. S. Couch, D. M. Greenblatt, E. C. Meng and T. E. Ferrin, UCSF Chimera—A visualization system for exploratory research and analysis, *J. Comput. Chem.*, 2004, **25**, 1605–1612.

74 M. M. Caldeira, M. L. Ramos, N. C. Oliveira and V. M. S. Gil, Complexes of vanadium(V) with α-hydroxycarboxylic acids studied by ^{1}H, ^{13}C, and ^{51}V nuclear magnetic resonance spectroscopy, *Can. J. Chem.*, 1987, **65**, 2434–2440.

75 A. Tracey, Applications of ^{51}V NMR spectroscopy to studies of the complexation of vanadium(V) by α-hydroxycarboxylic acids, *Coord. Chem. Rev.*, 2003, **237**, 113–121.

76 M.-H. Lee and I.-W. Kim, ^{13}C and ^{51}V Nuclear Magnetic Resonance Studies of Vanadium (δ)-α-Hydroxycarboxylate Complexes, *Bull. Korean Chem. Soc.*, 1993, **14**, 557–561.

77 A. Gorzsás, I. Andersson and L. Pettersson, Speciation in the aqueous $H^+/H_2VO_4^-/H_2O_2$/L -(+)-lactate system, *Dalton Trans.*, 2003, 2503–2511.

78 M. Biagioli, L. Strinna-Erre, G. Micera, A. Panzanelli and M. Zema, Molecular structure, characterization and reactivity of dioxo complexes formed by vanadium(V) with α-hydroxycarboxylate ligands, *Inorg. Chim. Acta*, 2000, **310**, 1–9.

79 B. Baruah, J. M. Roden, M. Sedgwick, N. M. Correa, D. C. Crans and N. E. Levinger, When Is Water Not Water? Exploring Water Confined in Large Reverse Micelles Using a Highly Charged Inorganic Molecular Probe, *J. Am. Chem. Soc.*, 2006, **128**, 12758–12765.

80 A. Gorzsás, K. Getty, I. Andersson and L. Pettersson, Speciation in the aqueous $H^+/H_2VO_4^-/H_2O_2$/citrate system of biomedical interest, *Dalton Trans.*, 2004, 2873–2882.

81 G. Ferraro, E. Garribba and A. Merlino, Exploring polyoxidovanadate–protein interaction, *Trends Chem.*, 2025, **7**, 3–6.

82 G. Tito, G. Ferraro, E. Garribba and A. Merlino, Formation of Mixed–Valence Cage–Like Polyoxidovanadates at 37 °C Upon Reaction of $V^{IV}O$(acetylacetonato)$_2$ With Lysozyme, *Chem. – Eur. J.*, 2025, **31**, e202500488.

83 C. Slebodnick and V. L. Pecoraro, Solvent effects on ^{51}V NMR chemical shifts: characterization of vanadate and peroxovanadate complexes in mixed water/acetonitrile solvent, *Inorg. Chim. Acta*, 1998, **283**, 37–43.

84 M. Aureliano and D. C. Crans, Decavanadate ($V_{10}O_{28}^{6-}$) and oxovanadates: Oxometalates with many biological activities, *J. Inorg. Biochem.*, 2009, **103**, 536–546.

85 H. T. Evans, Jr., The Molecular Structure of the Isopoly Complex Ion, Decavanadate ($V_{10}O_{28}^{6-}$), *Inorg. Chem.*, 1966, **5**(6), 967–977.

86 M. P. M. Marques, D. Gianolio, S. Ramos, L. A. E. Batista De Carvalho and M. Aureliano, An EXAFS Approach to the Study of Polyoxometalate–Protein Interactions: The Case of Decavanadate–Actin, *Inorg. Chem.*, 2017, **56**, 10893–10903.

87 F. Sun, Y.-T. Li, Z.-Y. Wu, D.-Q. Wang and J.-M. Dou, Tetrapiperidinium di-μ-methoxy-di-μ_5-oxo-tetra-μ_3-oxo-dodeca-μ_2-oxo-octaoxodecavanadate, *Acta Crystallogr., Sect. C:Cryst. Struct. Commun.*, 2006, **62**, m60–m62.

88 Y. Li, F. Sun, Z. Wu and Z. Zhang, Synthesis, Crystal Structure and Properties of Tetra(piperidinium)bis(ethanolate) Decavanadate, *Pol. J. Chem.*, 2007, **81**(8), 1379–1386.

89 T. Kiss, I. Sóvágó, R. B. Martin and J. Pursiainen, Ternary complex formation between Al(III)-adenosine-5′-phosphates and carboxylic acid derivatives, *J. Inorg. Biochem.*, 1994, **55**, 53–65.

90 T. Kiss, P. Buglyó, D. Sanna, G. Micera, P. Decock and D. Dewaele, Oxovanadium(IV) complexes of citric and tartaric acids in aqueous solution, *Inorg. Chim. Acta*, 1995, **239**, 145–153.

91 A. Merlino, Recent advances in protein metalation: structural studies, *Chem. Commun.*, 2021, **57**, 1295–1307.

92 M. F. A. Santos, I. Correia, A. R. Oliveira, E. Garribba, J. Costa Pessoa and T. Santos-Silva, Vanadium Complexes as Prospective Therapeutics: Structural Characterization of a V^{IV} Lysozyme Adduct, *Eur. J. Inorg. Chem.*, 2014, **2014**, 3293–3297.
93 D. Marasco, L. Messori, T. Marzo and A. Merlino, Oxaliplatin vs. cisplatin: competition experiments on their binding to lysozyme, *Dalton Trans.*, 2015, **44**, 10392–10398.
94 E. M. Phizicky and S. Fields, Protein-protein interactions: methods for detection and analysis, *Microbiol. Rev.*, 1995, **59**, 94–123.
95 I. M. A. Nooren, Diversity of protein-protein interactions, *EMBO J.*, 2003, **22**, 3486–3492.
96 A. Kapoor, S. Mondal, A. Chaudhary, S. Sharma, P. Mehra and A. Prasad, A topological review on protein–protein interactions: the development and promises in the era of omics, *J. Proteins Proteomics*, 2024, **15**, 523–544.
97 J. Janin and F. Rodier, Protein–protein interaction at crystal contacts, *Proteins:Struct., Funct., Bioinf.*, 1995, **23**, 580–587.
98 S. Ramos, M. Manuel, T. Tiago, R. Duarte, J. Martins, C. Gutiérrez-Merino, J. J. G. Moura and M. Aureliano, Decavanadate interactions with actin: Inhibition of G-actin polymerization and stabilization of decameric vanadate, *J. Inorg. Biochem.*, 2006, **100**, 1734–1743.